



Progress Towards the First High-Resolution Laser Spectroscopy of Exotic Fluorine Isotopes

Max Anton Gramberg*

Supervisors: Dr. Liss Vázquez Rodríguez^{†,‡}, Dr. Peter Plattner[‡]

June 16th – August 15th, 2025

*Department of Physics and Astronomy, Heidelberg University, Grabengasse 1, 69117 Heidelberg, Germany

[†]Max-Planck-Institut für Kernphysik, Saupfercheckweg 1, 69117 Heidelberg, Germany

[‡]ISOLDE, Experimental Physics Department, CERN, 1211 Geneva 23, Switzerland

Keywords: Collinear Laser Spectroscopy, ISOLDE, COLLAPS, Nuclear Properties

Summary The COLLAPS experiment aims to investigate exotic fluorine isotopes for the first time using high-resolution laser spectroscopy. To access these light-mass species, which have so far remained beyond experimental reach, a new technique is currently being implemented. This project, contributed to three different stages of the project. As a first step, the hyperfine spectra of the stable isotope (^{19}F) and that of ^{17}F : an expected proton-halo nucleus, have been simulated. As a second step, contributions to the preparations for a beamtime on the stable fluorine isotope – where some high-resolution laser spectroscopy has been performed – have been made. In closing the project, an active part could be taken in the first measurements with the new detection method, and some new insights into the level structure of ^{19}F could be gained by analysing the hyperfine spectra of the transitions surveyed in the beamtime.

1 Introduction

The COLLAPS¹ experiment, located at the ISOLDE² radioactive ion beam facility at CERN (Geneva), is a pioneering setup based on the technique of collinear laser spectroscopy (CLS).

The research focuses on the measurement of distinctive nuclear properties of short-lived and exotic radioactive nuclei. Properties such as the nuclear spin, electromagnetic moment, and charge radius of the nucleus itself influence the atomic energy levels and can be extracted by taking high-resolution optical spectra and investigating the tiny changes in the transition lines between the (fine structure) energy levels, i.e. the hyperfine structure and the isotope shift.

In the standard procedure of COLLAPS, the laser frequency is scanned and electrons are ex-

cited when the photon energy matches the energy difference between a lower and an upper hyperfine level. A resonantly induced optical transition causes photons to be absorbed and re-emitted. With high enough resolution the spectral fluorescent lines split into the hyperfine structure.

In the region of light nuclear masses (i.e. O and F), there are several interesting physics cases that are not or only hardly accessible with the standard CLS technique. Obstacles to overcome are transitions in the extreme ultra violet (XUV) regime, high chemical reactivities and/or low production yields (c.f. the original proposal [1]). Dedicated to the development of laser spectroscopy techniques with exceptional precision and sensitivity, there are currently ongoing efforts to commission a *state-selective re-ionisation* setup for the study of radioactive fluorine isotopes.

¹COLlinear LASer sPectroScopy

²Isotope Separator On Line DEvice

During my time at COLLAPS, I started with some simulations on the stable and the Fluorine isotope of interest, and their hyperfine spectra. For a large part of the project, I was involved in the preparations for a beamtime on the stable Fluorine isotope, which was meant as preparation for a radioactive beamtime in late November – to cover some technical details and to gain a better understanding of the different transitions. In the last weeks, I joint the commissioning of the test setup for the new measurement technique, took part in the beamtime and analysed the recorded data.

2 Simulations on $^{17,19}\text{F}$

For the simulation of the hyperfine structure of an atomic species, a couple of parameters have to be known, those are:

1. The total (electronic) angular momenta J of the states involved in the electronic transition. These can be found in the lower index of the term symbol $^{2S+1}L_J$, where S denotes the total spin and L the total orbital momentum of the electron configuration.

2. The nuclear spin I . This is dependent on the isotope and is usually known in beforehand. For very exotic isotopes the nuclear spin can be derived from the observed number of peaks in the spectrum.

3. The hyperfine parameters A and B . These constants characterise the coupling of the magnetic dipole moment and the electric quadrupole moment of the nucleus with the field created by the electrons. They are defined as

$$A = \frac{\mu_I B_J(0)}{I \cdot J} \quad (1)$$

and

$$B = e Q_s \cdot V_{JJ}(0), \quad (2)$$

where μ_I , the nuclear magnetic moment, may be known from NMR³ measurements, $B_J(0)$ is the magnetic field created by the electrons at the position of the nucleus and “is usually known from direct g_I -factor measurements” [2], e is the elementary charge, Q_s is the (spectroscopic) quadrupole moment and $V_{JJ}(0)$ is the electric field

³Nuclear Magnetic Resonance

gradient created by the electrons at the nucleus that “is taken from semi-empirical or theoretical analyses, unless precise values are available from the hfs of muonic atoms” [2].

4. The centroid of the hyperfine spectrum. This would be “the peak [frequency] for the isotope in the absence of hyperfine structure” [3], i.e. without a nuclear spin. Comparing centroid frequencies of different isotopes allows to measure isotope shifts and the deduction of differences in nuclear charge radii.

2.1 Isotope shifts

The isotope shift $\Delta\nu^{A,A'}$ of an optical transition is related to the perturbation of the atomic fine structure levels due to changes in the nuclear size and mass for varying isotopes. It is given by a sum of the mass- and field-shift contributions,

$$\begin{aligned} \Delta\nu^{A,A'} &= \nu^{A'} - \nu^A \\ &= F\delta\langle r^2 \rangle^{A,A'} + k_{\text{MS}} \frac{m_{A'} - m_A}{m_{A'} m_A}, \end{aligned} \quad (3)$$

with F being the field shift factor and k_{MS} the mass shift factor. $\delta\langle r^2 \rangle^{A,A'}$ is the difference in the nuclear mean square charge radius and $m_{A/A'}$ are the masses of the corresponding isotopes.

Bondarev has calculated the isotope shift factors for the $2p^4 3s^4 P_{5/2} \rightarrow 2p^4 3p^4 D_{5/2}^o$ transition in F I. His results for the field and mass shift factors are

$$\begin{aligned} F &= -22.4(5) \text{ MHz fm}^{-2} \\ \text{and } k_{\text{MS}} &= 264.7(23) \text{ GHz u} \end{aligned} \quad (4)$$

respectively [4]. He also performed an electronic structure calculations using a configuration interaction method, providing insight into the fields created by the electrons at the positions of the nucleus.

The nuclear charge radius of ^{19}F can be found in ‘Nuclear Charge Radii’ [5] so that together with the previous stated values for the isotope shift factors, all the quantities in eq. (3) are known to calculate the isotope shift between ^{19}F and ^{17}F , except the mean square nuclear charge radius of ^{17}F . This will be estimated in the following.

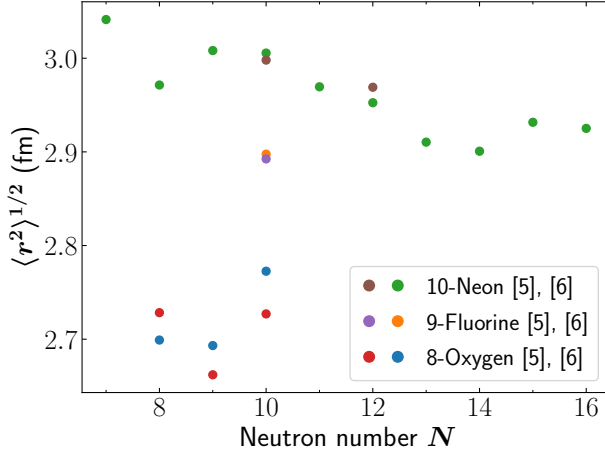


Figure 1: Tabulated root mean square nuclear charge radii of the elements around fluorine.

2.1.1 Nuclear charge radius of ^{17}F

The nuclear charge radius of ^{17}F is estimated from the trend of the nuclear charge radii of the neighbouring elements (oxygen and neon), as the nuclear charge radii of these elements are known over a broader range of isotopes. Figure 1 shows means of the tabulated root mean square (rms) nuclear charge radii from elastic electron scattering results $\langle r^2 \rangle_e^{1/2}$ of [5], where additionally – inspired by the *Live Chart of Nuclides* – more values from ‘Table of experimental nuclear ground state charge radii: An update’ [6] have been added.

Looking at the overall trend in the rms nuclear charge radii of the Neon isotopes, it seems that it could be approximated by a linear trend. Considering only the values at neutron numbers $N = 10$ and $N = 8$, the rms nuclear charge radii seems to make a step towards a lower value. Both extrapolations are depicted in Figure 2. The mean difference in the rms nuclear charge radius via the 2n-separation between neutron numbers 10 and 8 is approx. -0.0326 fm; the difference in the rms nuclear charge radius via the Neon trend is approx. 0.0262 fm. Despite this variance, the deviation of the two absolute values is still small:

2n-separation	2.8616 fm,
Neon trend	2.9204 fm,
relative difference	2.1 %.

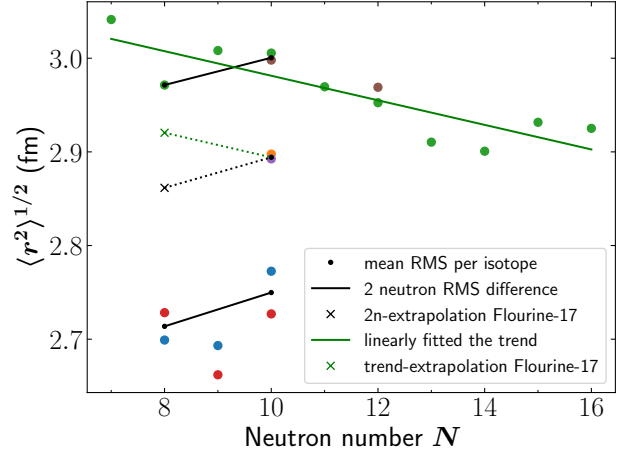


Figure 2: Extrapolation of the rms nuclear charge radius of ^{19}F for the estimation of the value of ^{17}F .

2.1.2 Isotope shift calculations

Taking the isotope masses from the 2020 Atomic Mass Evaluation [7] (referenced in the *Live Chart of Nuclides*), the isotope shift factors from eq. (4) and the deduced (rms) nuclear charge radius for ^{17}F – the isotope shift, eq. (3), can now be calculated and is (for the two extrapolation methods) given by:

2n-separation	1631.7 MHz,
Neon trend	1639.3 MHz.

2.2 HFS model of the $^4\text{P}_{5/2} \rightarrow ^4\text{D}_{5/2}$ transition

The transition of interest is the $2p^4 3s \ ^4\text{P}_{5/2} \rightarrow 2p^4 3p \ ^4\text{D}_{5/2}^o$ (electronic) transition in F I. The transition frequency of ^{19}F can be inferred from the energy levels indicated in *NIST, Atomic Spectra Database*, $102\,405.71\text{ cm}^{-1} \rightarrow 117\,164.01\text{ cm}^{-1}$. The total angular momentum J of the lower and the upper level involved is $5/2$ each. The nuclear spin I of ^{19}F is $1/2$, for ^{17}F it is $5/2$. The third set of parameters, the hyperfine parameters, and the centroid transition frequency of ^{17}F will be calculated in the following.

Table 1: Nuclear electromagnetic moments.

	¹⁹ F	¹⁷ F
μ_I (n.m.)	+2.628 321	+4.7213
Q_s (b)	0	0.076

Table 2: The magnetic field and the electric field gradient created by the electrons at the position of the nucleus.

Level	$B_J(0)/J$	$V_{JJ}(0) \cdot e$
$3s\ ^4P_{5/2}$	473	735
$3p\ ^4D_{5/2}$	213	171
Unit	MHz/n.m.	MHz/b

2.2.1 Calculating the hyperfine parameters

For the calculation of the A 's and B 's, the recommended nuclear electromagnetic moments from the database *Nuclear Electromagnetic Moments* [8] based on the *Nuclear moments tables* [9, 10] are used. The corresponding values are given in Table 1.

The nuclear magnetic moment μ_I is given in nuclear magneton μ_N (n.m.) and the quadrupole moment Q_s in barn (b).

The fields created by the electrons at the position of the nucleus are taken from [4], noticing that $B_J(0)/J = \frac{\mathcal{A}_{\text{hfs}}}{\mu_I/I} = \mathcal{A}_{\text{hfs}}/g_I$ and $V_{JJ}(0) \cdot e = \mathcal{B}_{\text{hfs}}/Q_s$. Calling the $^4P_{5/2}$ the *lower* state and the $^4D_{5/2}$ the *upper* state, the “normalised” values of the magnetic field and the electric field gradient are given in Table 2.

The theory values of the hyperfine parameters can be easily calculated from these numbers, using eqs. (1) and (2). In addition, more accurate, experimental values for the hyperfine parameter A in ¹⁹F can be extrapolated to the values in ¹⁷F, using the following relation [11, p. 616]:

$$\frac{A}{A_{\text{ref}}} = \frac{\mu_I/I}{(\mu_I/I)_{\text{ref}}} \longrightarrow A = A_{\text{ref}} \frac{I_{\text{ref}}}{\mu_{I,\text{ref}}} \frac{\mu_I}{I}. \quad (5)$$

The experimental values for the hyperfine parameter A_{ref} in ¹⁹F are taken from [12] and a summary of all (calculated) values is given in Tables 3 and 4.

Table 3: Hyperfine structure parameters in ¹⁹F I.

¹⁹ F	Hyperfine constant (MHz)		
	A_{theo}	A_{exp}	B_{theo}
$3s\ ^4P_{5/2}$	+2486	+2643(1)	0
$3p\ ^4D_{5/2}$	+1120	+1148(1)	0

Table 4: Hyperfine structure parameters in ¹⁷F I.

¹⁷ F	Hyperfine constant (MHz)		
	A_{theo}	A_{ext}	B_{theo}
$3s\ ^4P_{5/2}$	+893.3	+949.5	55.86
$3p\ ^4D_{5/2}$	+402.3	+412.4	13.00

2.2.2 Centroid transition frequency of ¹⁷F

The centroid frequency of the transition of interest in ¹⁹F I is available from spectroscopic data and the (experimental) values are taken from [13]. For ¹⁷F, the centroid frequency is calculated from the isotope shift between ¹⁷F and ¹⁹F, calculated in section 2.1.2. The two extrapolation methods (2n-separation and Neon trend) only deviate by 7.6 MHz and it is likely that they cannot be distinguished in the spectra. The centroid frequency is calculated from the mean of the two calculated isotope shifts:

$$\Delta\bar{\nu}^{19,17} = 1635.5 \text{ MHz}.$$

The centroid transition frequencies are listed in Table 5 in different units.

Table 5: Centroid frequency of the transition of interest in the two isotopes and in different units.

$3s\ ^4P_{5/2} \rightarrow 3p\ ^4D_{5/2}$		
F I	ν^{19}	$\bar{\nu}^{17}$
in THz	442.442 344	442.443 979
in nm	677.585 368	677.582 863
in cm ⁻¹	14 758.288 [13]	14 758.343

2.2.3 Simulated hyperfine spectra

All the information gathered up to this point can now be fed into functions of SATLAS2⁴: a Python library that enables to model and to fit counting data from laser spectroscopy experiments, in particular made for those that measure atomic hyperfine structures [14].

Each spectrum is modelled twice, thereby comparing the calculated (theoretical) and measured (experimental) values of the hyperfine parameters (Figures 3 and 4). In the case of ¹⁷F, both isotopic shifts are indicated in the plots to show the vanishing difference between the two extrapolation methods (2n-separation and Neon trend; see esp. Figure 5).

2.2.4 Scanning range calculation

In their rest frame, the moving atoms experience the laser from the laboratory at frequency ν_{lab} at a shifted frequency ν . To scan through the atomic spectrum, not the laser itself but the acceleration voltage of the ions is varied, before they undergo neutralisation.

Knowing the frequency range of the full spectrum, the range of the scanning voltage can be calculated as follows:

1. Calculate the beta-factor ($\beta = v/c$) for the simulated detuning from the lab-laser frequency:

$$\beta = \frac{1 - (\nu/\nu_{\text{lab}})^2}{1 + (\nu/\nu_{\text{lab}})^2}. \quad (6)$$

2. With the velocity $v = \beta c$, calculate the kinetic energy of the atoms:

$$E = \frac{1}{2} m_A v^2. \quad (7)$$

3. The scanning voltage U is an additional accelerating/retarding voltage to the normal acceleration U_0 and can then be calculated from:

$$U = U_0 - E/e, \quad (8)$$

where e is the elementary charge.

The lab-laser frequency ν_{lab} is commonly chosen such that the centroid of the spectrum,

⁴Statistical Analysis Toolbox for LAser Spectroscopy, version 2

ν_{ref} appears at zero scanning voltage ($U = 0$ V). It can be calculated using the following relations:

$$E_{\text{ref}} = eU_0, \quad (9)$$

$$v_{\text{ref}} = \sqrt{2E_{\text{ref}}/m_A} \quad \text{and} \quad \beta_{\text{ref}} = v_{\text{ref}}/c, \quad (10)$$

$$\nu_{\text{lab}} = \nu_{\text{ref}} \div \sqrt{\frac{1 - \beta_{\text{ref}}}{1 + \beta_{\text{ref}}}}. \quad (11)$$

Figure 6 shows the hyperfine spectra of the two isotopes ($A = 19, 17$) – in the scanning voltage frame – on top of each other. ν_{lab} is fixed at an arbitrary frequency such that both spectra lie within the same scanning range, demonstrating the mass dependence of the Doppler effect, as the spectra are more literally on top of each other in the frequency frame (cf. Figure 3 to 4).

3 Setup Preparation for Stable-Ions Beamtime

In preparation for the beamtime on the stable Fluorine isotope (¹⁹F), some changes had to be made on the setup, in particular on the optical detection region. Afterwards, the optical alignment of the setup has to be restored.

The photomultiplier tubes (PMTs) had to be interchanged. The infrared-sensitive PMTs needed to be mechanically integrated and for the reduction of their dark count rate, they need to be cooled. The latter has been implemented with an cooling thermostat, using ethanol as a cooling liquid. Reaching temperatures $< 10^\circ\text{C}$ requires proper isolation of the connecting lines, and the evacuation of the inside of the detectors to avoid condensation, especially on the optical elements.

The alignment of the laser and the beamline itself has been adjusted to minimise laser-induced stray light on the PMTs. To further improve the signal-to-noise ratio (S/N), count rates have been measured for the optimisation of the bias voltage of the PMTs, which is described in the following.

3.1 Optical detection optimisation

Measuring the background count rate when the laser is turned on or off (un-/blocked) at varying bias voltage allows to tune the S/N ratio.

Acquisition of the count rates with the laser turned off $R_{\text{L,off}}$ or on $R_{\text{L,on}}$, allows to deduce

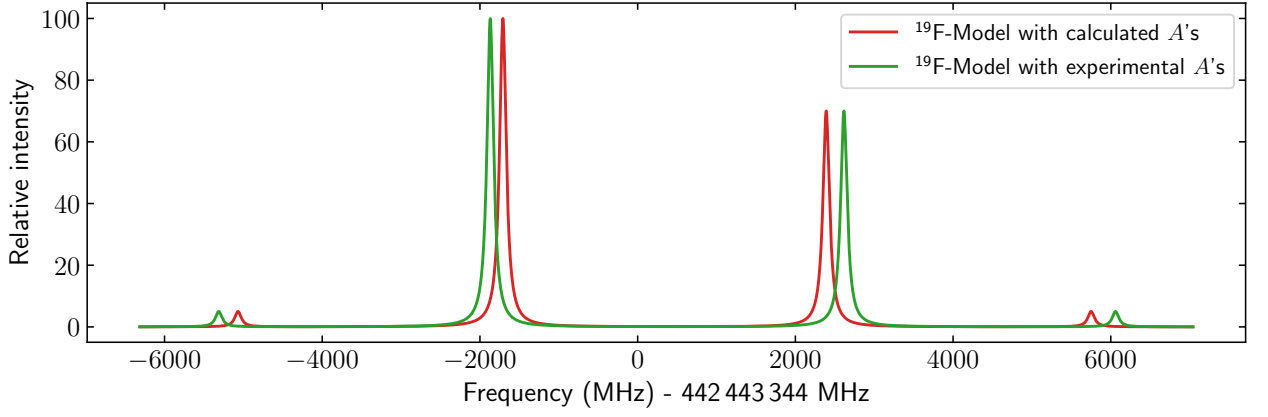


Figure 3: Simulated hyperfine spectrum of the $^4P_{5/2} \rightarrow ^4D_{5/2}$ transition in ^{19}F .

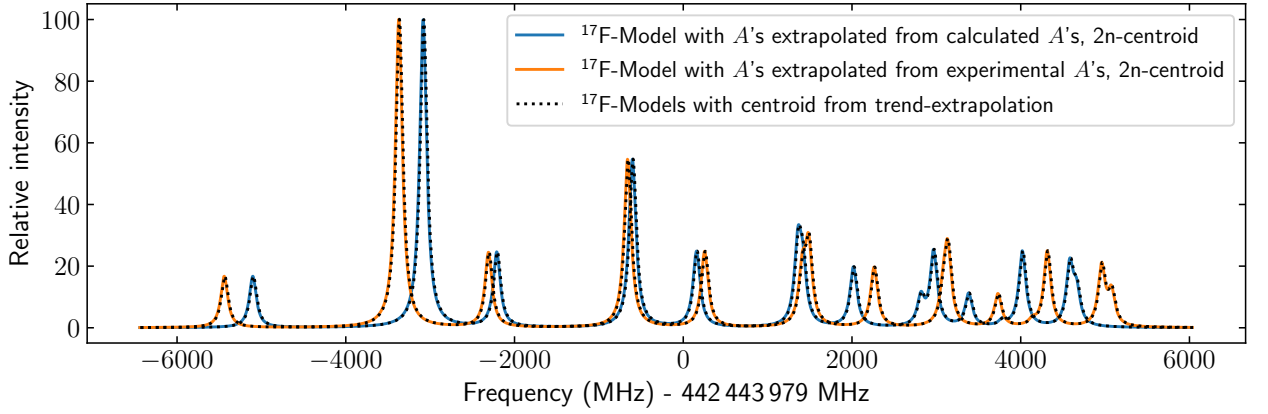


Figure 4: Simulated hyperfine spectrum of the $^4P_{5/2} \rightarrow ^4D_{5/2}$ transition in ^{17}F .

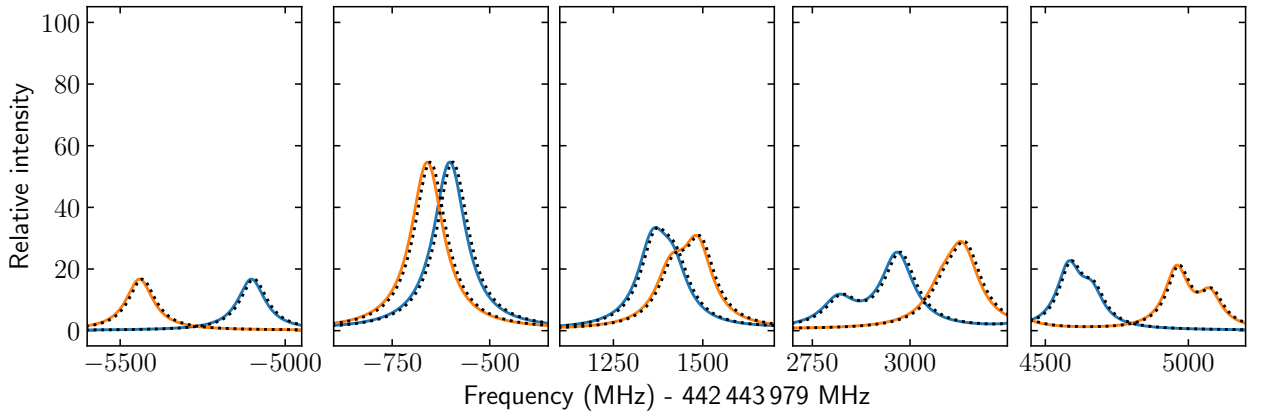


Figure 5: Details of the ^{17}F spectrum.

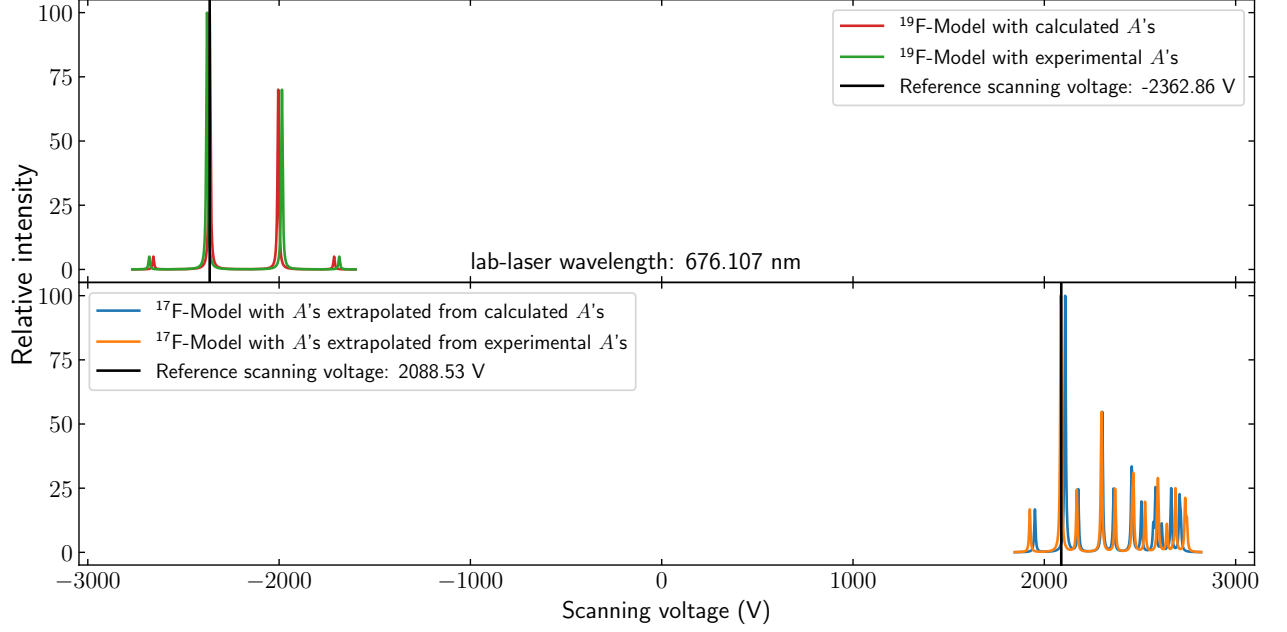


Figure 6: Scanning voltage spectra.

several measures, which are related as follows:

$$\begin{aligned} R_{L,\text{off}} &= B, & R_{L,\text{on}} &= S + B, \\ S &= R_{L,\text{on}} - R_{L,\text{off}}, & S/N &= S/\sqrt{B}. \end{aligned} \quad (12)$$

Here, B is the background rate, S is the signal rate, N is the noise rate and S/N or S/B are the signal-to-noise or the signal-to-background ratio.

Depicted in Figure 7 are the different count rates as a function of bias voltage. Each column displays the data of one of four PMTs. They may have a different working point, but should be operated at a bias voltage below 2300 V [15].

The rates $R_{L,\text{off}}$, $R_{L,\text{on}}$ and S follow approximately typical voltage gain characteristics (close to

linear but understating at higher values; see e.g. [15, item 7]). In most instances, broad steps were chosen when turning the bias up, and additional points have been taken when again turning the bias down. These do not always tally the previously measured rate, but are sometimes offset to them – thought to be due to changes in the laser power as it can be mainly observed in $R_{L,\text{on}}$.

Still, while the three rates depicted at the top keep increasing with bias, the ratios S/B and S/N start levelling off at higher bias and depending on the PMT there is a more or less pronounced decrease afterwards. This allows an optimised bias value to be selected.

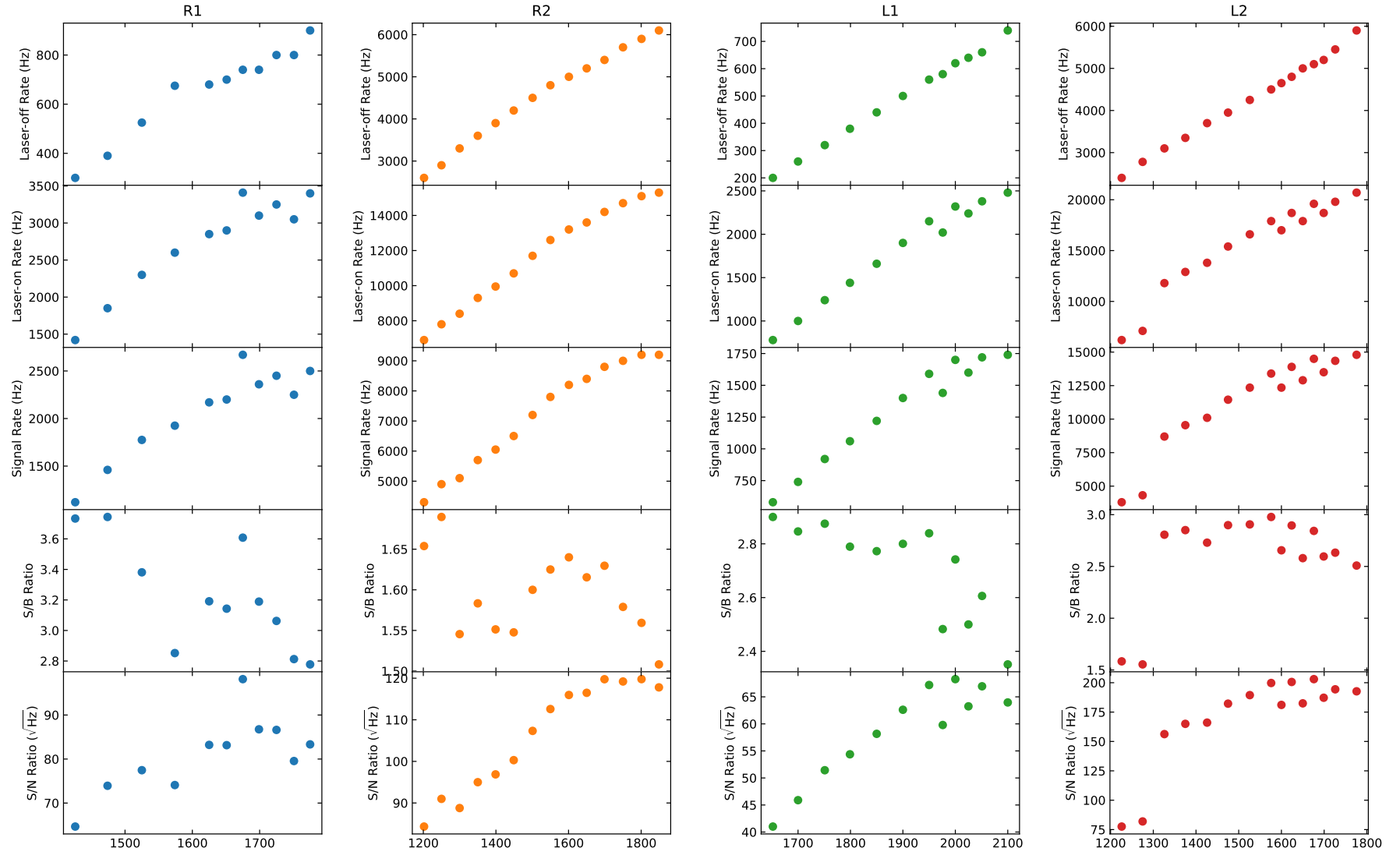


Figure 7: Measurements of the background and signal rates for the determination of an optimised bias value.

4 Beamtime

4.1 Summary

The beamtime on the stable Fluorine isotope (^{19}F) has been carried out from 31/07 to 03/08 2025. It served the purpose of 1. gaining some more insight into a. the shape of the ion beam coming from the general purpose separator (GPS) of the ISOLDE facility, b. the tunability of the beam size; 2. characterising the neutralisation efficiency of the charge-exchange-cell and 3. performing some high-resolution laser spectroscopy on ^{19}F .

Three different transitions have been studied thereby probing the hyperfine parameter A of four different levels. The data analysis is presented in the following.

4.2 Data analysis

4.2.1 Readout and pre-processing of the data

The transitions have been scanned by means of 3 to 4 *high-resolution scans* that consist of a set number of *runs* (10 in most cases). In each run, the spectrum is divided into its relevant features, so called “**tracks**”, thereby skipping sections that only contain the baseline and no (peak) signals. These are scanned several times (5 to 10 *scans* for tracks with small peaks, 2 *scans* for tracks with large peaks). The different (sub-)units of the measurements will later be called “**HRES scan**”, “**run**” and “**scan**”. For each run, the tracks are available for each of the four PMTs separately.

When reading out the data, the logged data of the high-voltage of the ISOLDE target⁵ (target HV) and the wavemeter reading of the frequency of the laser in the laboratory are reviewed. During some runs, the target HV jumped (only by $\sim 0.4\text{ V}$ out of the $\sim 30\text{ kV}$ acceleration voltage, but still) and/or the frequency of the laser drifted.

For each transition, the data is read out per HRES scan. Runs with too large fluctuations

⁵The extraction voltage of the ion source where the radioactive isotopes are created by the 1.4 GeV proton beam from the Proton Synchrotron Booster being directed onto a specially developed “thick” target.

of the target HV or the laser frequency are neglected. All other runs are first averaged per PMT and then the data of the PMTs with a good S/N are summed resulting in the final spectrum of one HRES scan. As a result, three (or four) high-statistics spectra remain – per transition – for further analysis.

4.2.2 Voltage calibration

The recorded spectra initially show the signal intensity (in counts) as a function of the line voltage, i.e. a voltage in the range of -1 V to $+1\text{ V}$ that is fed to a high voltage amplifier whose outgoing signal, the scanning voltage, modifies the energy of the ion beam prior to neutralisation (in the range of -1 kV to $+1\text{ kV}$).

Prior to the actual (or rather the scientific) data taking, a read-back of the scanning voltage is measured as a function of the line voltage. The read-back is the scanning voltage scaled down with a voltage divider that has a divider ratio of 1000.02(7) – the average of two calibration measurements. The relationship between the read-back and the line voltage is given by a linear function of type $y = a \cdot x + b$ with $a = 1.000\,666\,4(5)$ and $b = 0.000\,108\,31(26)$ prior to the first measured spectra. The fit and the residuals are given in Figures 11 and 12 in the Appendix. The calibration was repeated between the second and third transition.

Knowing the real scanning voltage and the laser frequency as logged by a HighFinesse WS10 wavemeter in the lab, one can calculate the laser frequency in the rest frame of the atoms (cf. section 2.2.4).

The summation of sets of runs as described at the end of the last section (4.2.1) together with a transformation of units (from *line voltage* to *detuning from COG laser frequency*) is shown in the Appendix in Figure 13).

4.2.3 Fitting the spectra with SATLAS2 models

To simultaneously fit the HRES scans of each transition, the hyperfine spectrum model has to be setup: The nuclear spin, the (electronic) angular momentum of the upper and lower level,

Table 6: Fitting model parameters.

Parameter	Options (resp. variables)
background	constant; linear (sloped)
lineshape	Voigt; skewed Voigt
sidepeaks	number $N \in \{0, 1, 2, 3\}$ (+ offset, poisson factor)

initial guesses of the hyperfine parameter A ($B = 0$ for this isotope), and initial guesses of the linewidth and centroid position have to be set. The scale of the spectrum is estimated as well as the magnitude of the background (noise) level. Moreover, the lineshape that is fitted to the peaks can be set/chosen.

Models that were used to try to improve the fit result comprise fits with different combinations of the parameters listed in Table 6. It was found that a fit with a sloped background, a skewed voigt and one (single) sidepeak provides the best fit results (lowest [reduced] chi-squared). The fits and the values yielded are shown in Figures 8 to 10 and the hyperfine parameters are summarised and compared in Table 7. The results of a fit with a pure Voigt lineshape are tabulated to show the improvement obtained.

5 Outlook

In the week of the beamtime, some first *state selective collisional ionisation* measurements could be carried out within the LIAF⁶ group, thereby commissioning the test setup for this technique

⁶i.e. the Laboratory for Laser Induced Atomic Fluorescence and ionization.

in an offline laboratory. At a later stage, this will be transferred and connected to the COLLAPS experiment.

For the next beamtime on the radioactive Fluorine isotope (^{17}F), this much more sensitive technique will be needed. The production yield for the isotope is so low that spectra cannot be taken with the standard fluorescence based photon-counting, but should be easily resolvable with this ion counting technique, if there is no major background contamination of other re-ionisable elements.

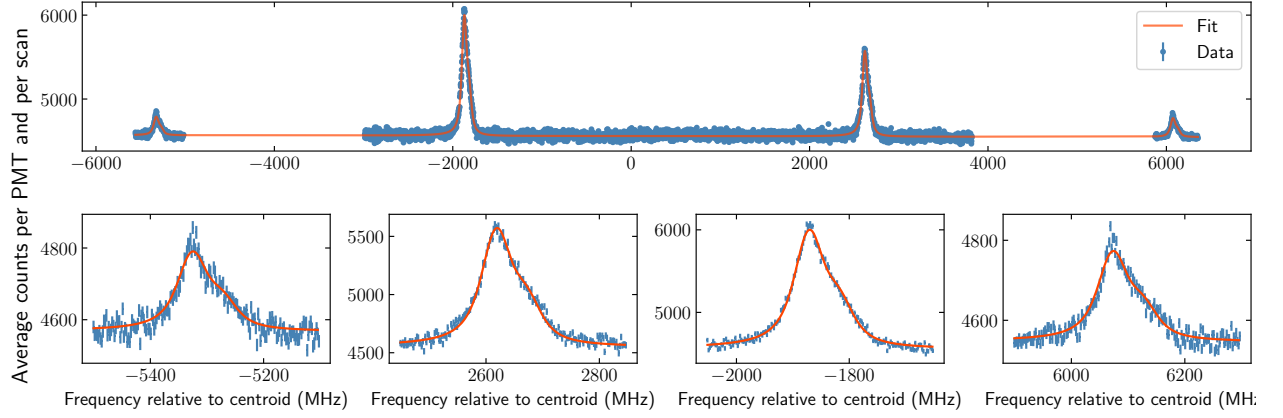
Acknowledgments

I would like to express my sincere gratitude to my supervisors, Liss V. Rodríguez and Peter Plattner, for welcoming me into her team and his office, respectively, and for their expert guidance, support and co-operation throughout this project. I would also like to thank all the other COLLAPS locals for the joint work and the wonderful time spent together during breaks and in the heat.

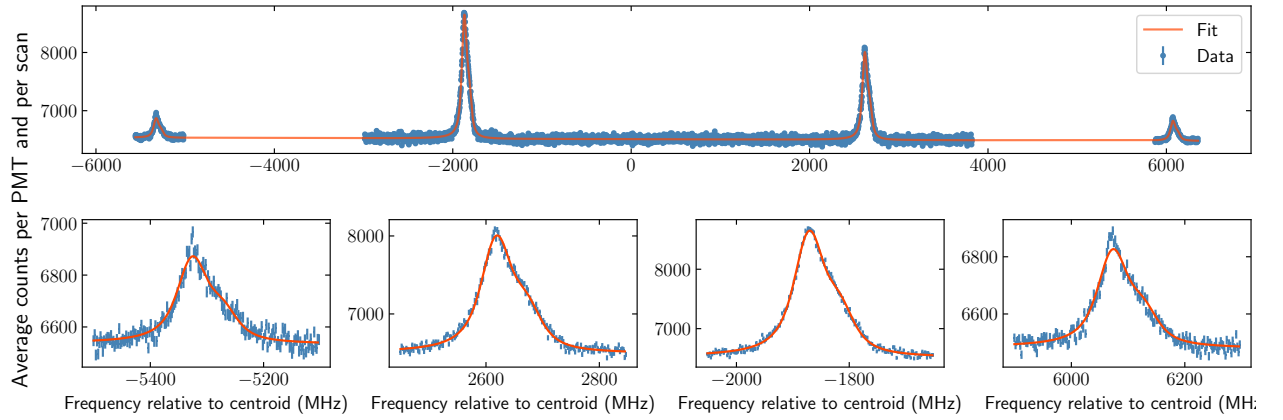
My time at CERN was an incredible and unforgettable experience, thanks to all the wonderful people I met there.

Table 7: Summary of the extracted hyperfine parameters.

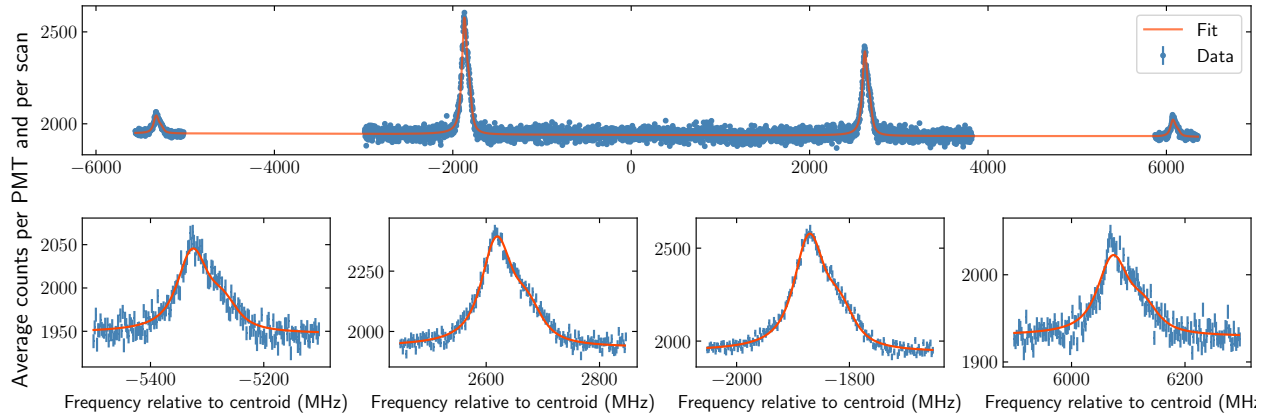
	state/level	Literature [12]	Pure Voigt fit	Best fit (1 Sidepeak + skew)
A_u	$3p\ ^4D_{5/2}$	1148(1)	1151.49(13) 1151.41(15)	1151.52(11) 1151.33(12) } 1151.43(8)
	$3p\ ^4D_{7/2}$	1564(1)	1566.98(18)	1566.71(8)
A_l	$3s\ ^4P_{3/2}$	—	502.60(23)	502.52(18)
	$3s\ ^4P_{5/2}$	2643(1)	2648.02(13) 2648.28(24)	2648.05(11) 2647.99(11) } 2648.02(8)



(a) Sum of runs 29 to 35; Centroid: 442 443 574.16(27) MHz; FWHMG: 21.1(12) MHz; FWHML: 49.2(12) MHz



(b) Sum of runs 36 to 45; Centroid: 442 443 574.07(24) MHz; FWHMG: 22.1(10) MHz; FWHML: 48.4(10) MHz



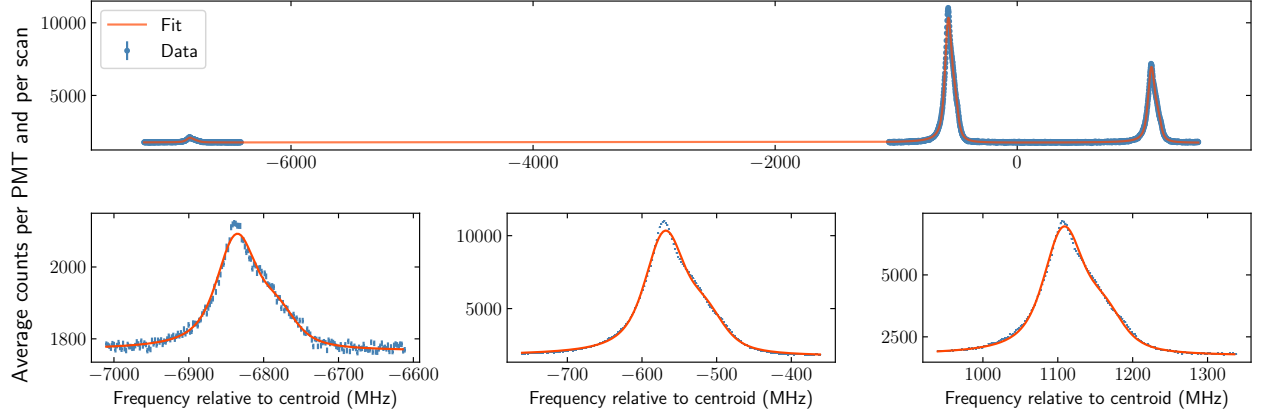
(c) Sum of runs 46 to 48; Centroid: 442 443 574.26(36) MHz; FWHMG: 20.0(17) MHz; FWHML: 50.8(16) MHz

Figure 8: High-resolution hyperfine spectra of the $^4\text{P}_{5/2} \rightarrow ^4\text{D}_{5/2}$ transition in ^{19}F ($I = 1/2$).

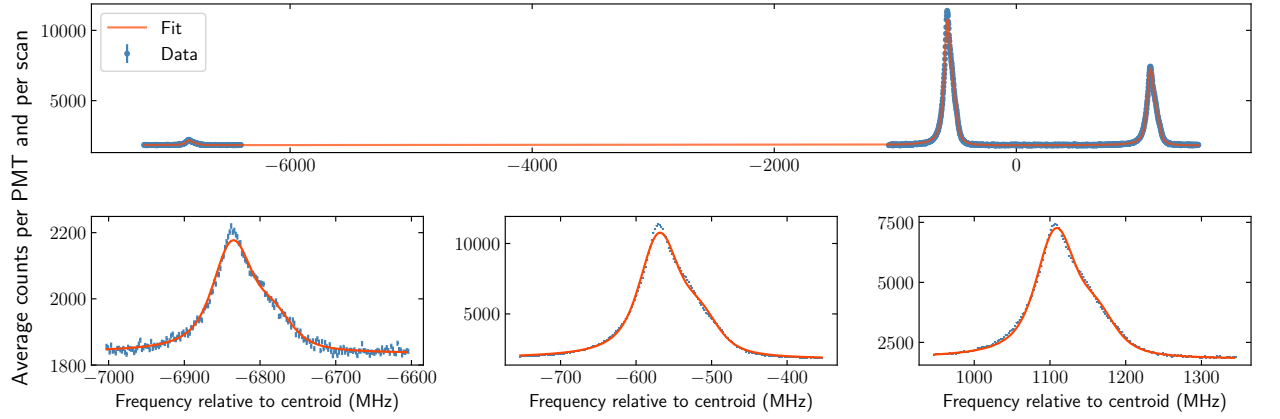
Shared fitting parameters: $A_l = 2648.05(11)$ MHz; $A_u = 1151.52(11)$ MHz; skew = $-0.039(5)$; Sidepeaks $N = 1$ (fixed); Offset = $53.6(4)$; Poisson = $0.338(7)$.

Mean centroid frequency: 442 443 574.16(19) MHz.

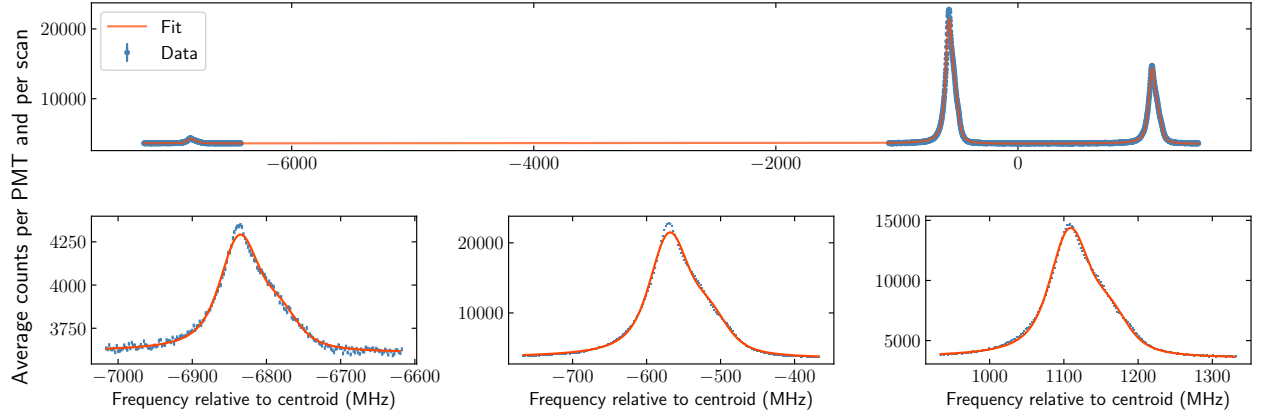
Fit Statistics: fitting method: least squares; $\chi^2 = 16\,156$; $\chi^2_{\text{red.}} = 1.43$;
data points = 11 316; # variables = 32.



(a) Sum of runs 63 to 65; Centroid: 437 149 075.26(11) MHz; FWHMG: 26.3(4) MHz; FWHML: 40.8(4) MHz



(b) Sum of runs 73 to 75; Centroid: 437 149 076.28(11) MHz; FWHMG: 25.7(4) MHz; FWHML: 40.1(4) MHz



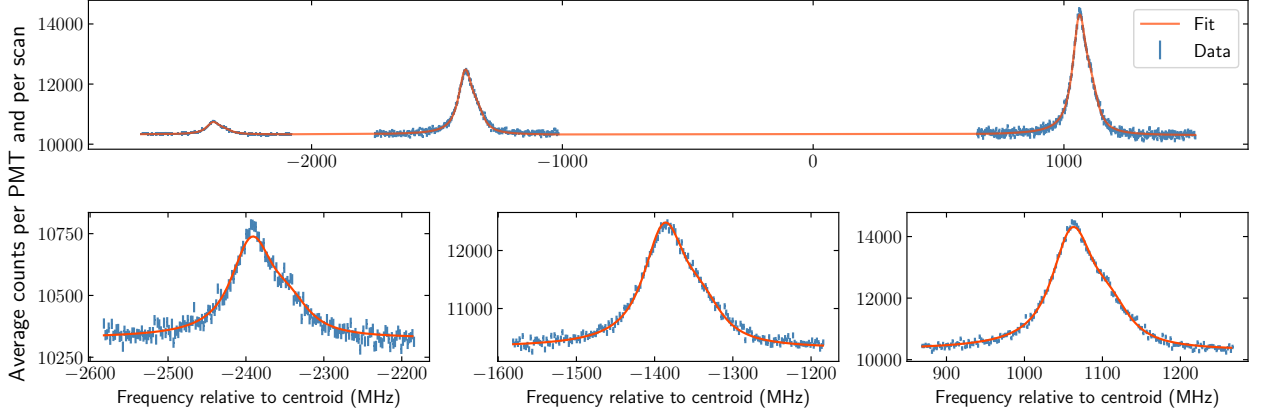
(c) Sum of runs 84 to 89; Centroid: 437 149 075.94(9) MHz; FWHMG: 26.53(28) MHz; FWHML: 40.3(3) MHz

Figure 9: Hyperfine spectrum of the $^4\text{P}_{5/2} \rightarrow ^4\text{D}_{7/2}$ transition in ^{19}F ($I = 1/2$).

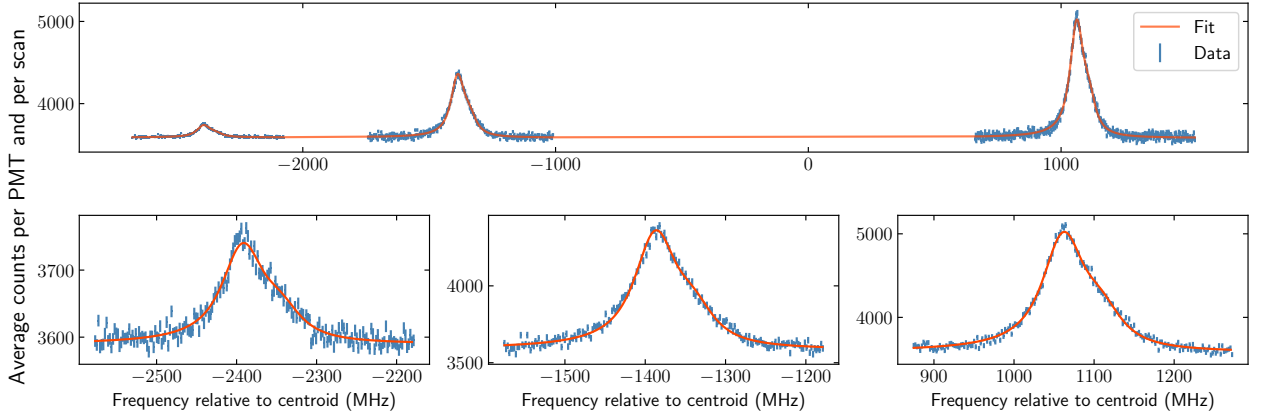
Shared fitting parameters: $A_l = 2647.99(11)$ MHz; $A_u = 1566.71(8)$ MHz; skew = $-0.0790(22)$; Sidepeaks $N = 1$ (fixed); Offset = $53.32(16)$; Poisson = $0.3145(23)$.

Mean centroid frequency: 437 149 075.8(4) MHz.

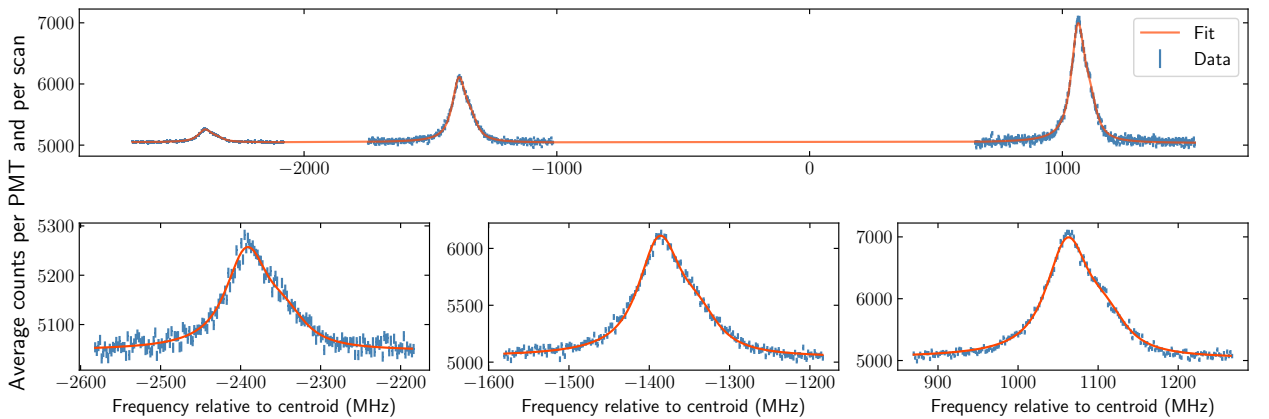
Fit Statistics: fitting method: least squares; $\chi^2 = 36\,925$; $\chi^2_{\text{red.}} = 7.5$;
data points = 4923; # variables = 29.



(a) Sum of runs 110 to 129; Centroid: 434 207 383.31(26) MHz; FWHMG: 14.6(14) MHz; FWHML: 56.1(11) MHz

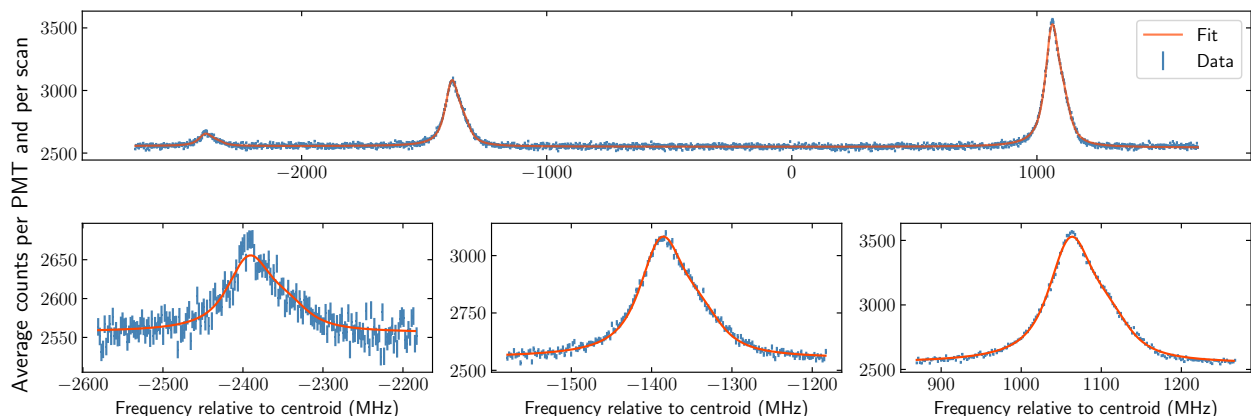


(b) Sum of runs 133 to 139; Centroid: 434 207 382.78(30) MHz; FWHMG: 12.6(15) MHz; FWHML: 56.8(11) MHz



(c) Sum of runs 140 to 149; Centroid: 434 207 382.68(26) MHz; FWHMG: 15.3(14) MHz; FWHML: 54.9(11) MHz

Figure 10: Hyperfine spectrum of the $^4\text{P}_{3/2} \rightarrow ^4\text{D}_{5/2}$ transition in ^{19}F ($I = 1/2$).



(d) Sum of runs 101 to 105; Centroid: 434 207 382.13(21) MHz; FWHMG: 20.2(10) MHz; FWHML: 51.8(9) MHz

Figure 10 (cont.): Hyperfine spectrum of the $^4\text{P}_{3/2} \rightarrow ^4\text{D}_{5/2}$ transition in ^{19}F ($I = 1/2$).

Shared fitting parameters: $A_l = 502.52(18)$ MHz; $A_u = 1151.33(12)$ MHz; skew = $-0.026(3)$; Sidepeaks $N = 1$ (fixed); Offset = $47.1(4)$; Poisson = $0.293(6)$.

Mean centroid frequency: 434 207 382.73(45) MHz.

Fit Statistics: fitting method: least squares; $\chi^2 = 7292$; $\chi^2_{\text{red.}} = 1.36$;
data points = 5383; # variables = 37.

References

- [1] Garcia Ruiz and Ronald Fernando. *Towards laser spectroscopy of exotic fluorine isotopes*. CERN-INTC-2016-037, INTC-I-171. Geneva: CERN, 2016. URL: <https://cds.cern.ch/record/2157183>.
- [2] R Neugart. ‘Collinear fast-beam laser spectroscopy’. In: *Prog. At. Spectr., D* (1987), pp. 75–126. URL: <https://cds.cern.ch/record/178647>.
- [3] B. White, N. C. M. Bulstrode, D. H. Forest, C. Honeyball, B. Evans and L. Butt. ‘Spin assignment, hyperfine structure, and isotope shift measurements of optical transitions in dysprosium I’. In: *Journal of Physics B: Atomic, Molecular and Optical Physics* 58.3 (Jan. 2025), p. 035001. DOI: [10.1088/1361-6455/adacbe](https://doi.org/10.1088/1361-6455/adacbe).
- [4] Andrey Bondarev. ‘Calculations of isotope shift factors in F I’. Internal communication. 30th Apr. 2025.
- [5] G. Fricke and K. Heilig. ‘Nuclear Charge Radii’. In: *Landolt-Börnstein - Group I Elementary Particles, Nuclei and Atoms*. Ed. by H. Schopper. Vol. 20. Landolt-Börnstein: Numerical Data and Functional Relationships in Science and Technology - New Series. Berlin, Heidelberg: Springer, 2004. DOI: [10.1007/10856314_11](https://doi.org/10.1007/10856314_11).
- [6] I. Angeli and K.P. Marinova. ‘Table of experimental nuclear ground state charge radii: An update’. In: *Atomic Data and Nuclear Data Tables* 99.1 (2013), pp. 69–95. DOI: [10.1016/j.adt.2011.12.006](https://doi.org/10.1016/j.adt.2011.12.006).
- [7] Meng Wang, W.J. Huang, F.G. Kondev, G. Audi and S. Naimi. ‘The AME 2020 atomic mass evaluation (II). Tables, graphs and references’. In: *Chinese Physics C* 45.3 (Mar. 2021), p. 030003. DOI: [10.1088/1674-1137/abddaf](https://doi.org/10.1088/1674-1137/abddaf).
- [8] International Atomic Energy Agency - Nuclear Data Section. *Nuclear Electromagnetic Moments*. <https://www-nds.iaea.org/nuclearmoments/>. 2014. (Visited on 19/06/2025).
- [9] N.J. Stone. *Table of Recommended Nuclear Magnetic Dipole Moments: Part I - Long-lived States*. INDC(NDS)-0794. Vienna: International Atomic Energy Agency - Nuclear Data Section, Nov. 2019. DOI: [10.61092/iaea.yjpc-cns6](https://doi.org/10.61092/iaea.yjpc-cns6).

- [10] N.J. Stone. *Table of Nuclear Electric Quadrupole Moments*. INDC(NDS)-0794. Vienna: International Atomic Energy Agency - Nuclear Data Section, Oct. 2021. DOI: [10.61092/iaea.a6te-dg7q](https://doi.org/10.61092/iaea.a6te-dg7q).
- [11] Kenneth S. Krane. *Introductory nuclear physics*. Rev. ed. New York [u.a.]: Wiley, 1988.
- [12] C.D.P. Levy, T.E. Cocolios, J.A. Behr, K. Jayamanna, K. Minamisono and M.R. Pearson. ‘Feasibility study of in-beam polarization of fluorine’. In: *Nuclear Instruments and Methods in Physics Research Section A: Accelerators, Spectrometers, Detectors and Associated Equipment* 580.3 (2007), pp. 1571–1577. DOI: [10.1016/j.nima.2007.07.013](https://doi.org/10.1016/j.nima.2007.07.013).
- [13] A. Kramida, Yu. Ralchenko, J. Reader and NIST ASD Team. *NIST Atomic Spectra Database*. Version 5.12. Gaithersburg, MD: National Institute of Standards and Technology, 2024. DOI: [10.18434/T4W30F](https://doi.org/10.18434/T4W30F). Available: <https://physics.nist.gov/asd> (Online). (Visited on 20/06/2025).
- [14] W. Gins, B. van den Borne, R.P. de Groote and G. Neyens. ‘SATLAS2: An update to the package for analysis of counting data’. In: *Computer Physics Communications* 297 (2024), p. 109053. ISSN: 0010-4655. DOI: [10.1016/j.cpc.2023.109053](https://doi.org/10.1016/j.cpc.2023.109053). Documentation: <https://iksnm.github.io/satlas2/>.
- [15] *9658B series data sheet*. Issue 6. ET Enterprises, Ltd. Uxbridge, United Kingdom, Apr. 2015. URL: https://et-enterprises.com/images/data_sheets/9658B.pdf (visited on 23/07/2025).

Appendix

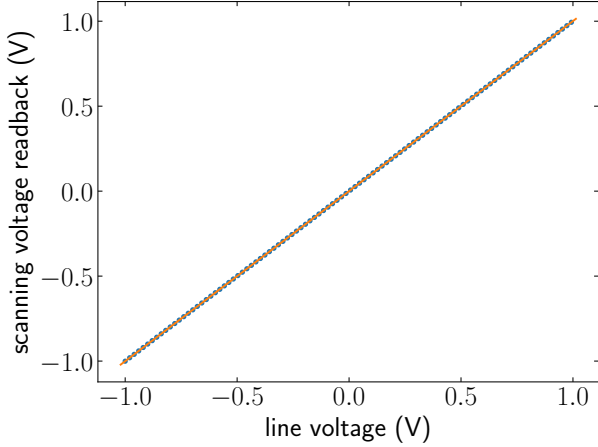


Figure 11: Voltage calibration fit (example).

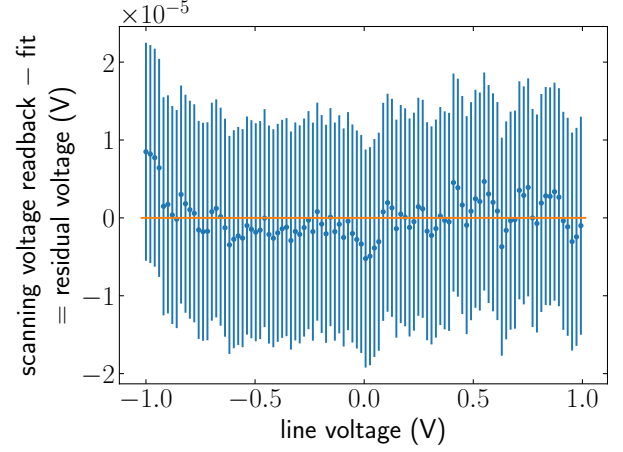


Figure 12: Voltage calibration residuals (example).

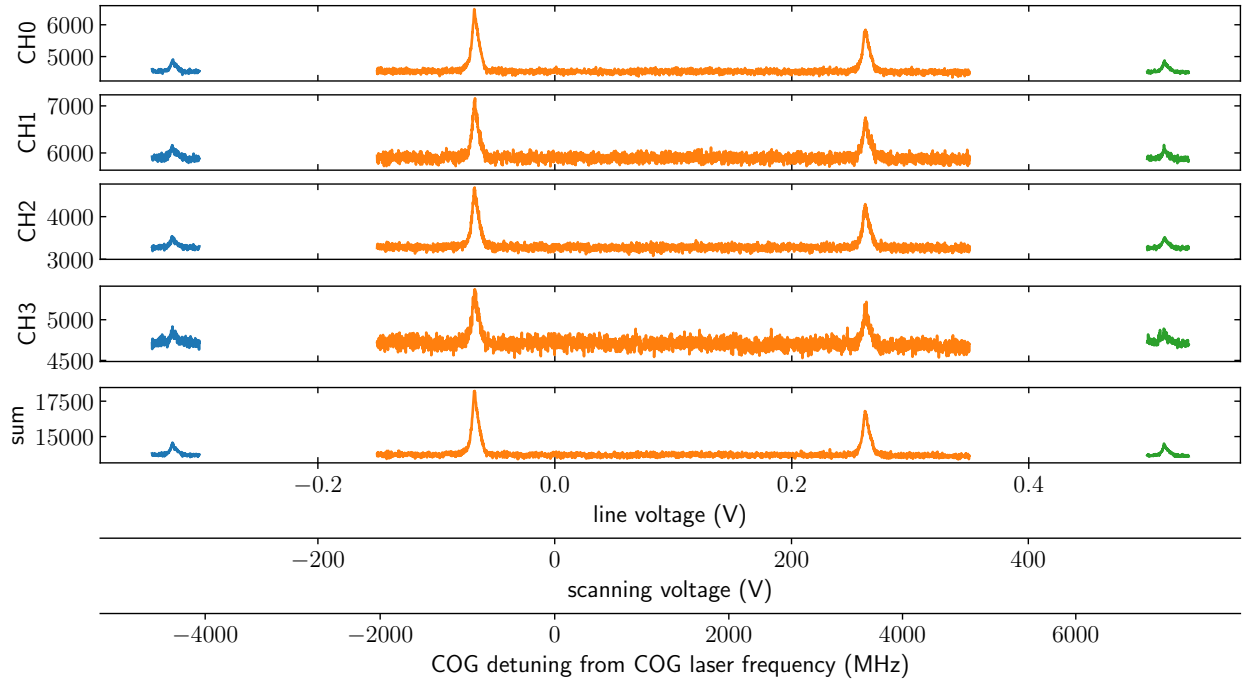


Figure 13: Summing sets of runs and unit conversion. In this example, only the channels 0, 1 and 2 are used for the sum, as channel three was considered to be too noisy. For the subsequent analysis, the summed counts are divided by the number of channels (PMTs) to get a value for the *average counts per PMT and per scan*.